Proceedings of ICBioMed 2025 Symposium: AI for Healthcare: Advanced Medical Data Analytics and Smart Rehabilitation
DOI: 10.54254/2753-8818/2025.AU27980

Opposing Climate–Malaria Correlations in West and East Africa: Temperature and Rainfall Effects Vary by Region

Haoming Li[1*], Minjie Yuan[2], Yu Tang[3]

[1]Department of Mathematics, University of Rochester, New York, USA
[2]Department of Biology, University of Rochester, New York, USA
[3]Shanghai New Hongqiao High School, Shanghai, China
**Corresponding Author Email: hli103@u.rochester.edu*

Abstract. Malaria remains a critical health challenge in Africa, where transmission is shaped by climatic variability. This study examines the joint effects of temperature and rainfall on malaria incidence, mortality, and infection prevalence across African countries (2010–2015) using data from the Malaria Atlas Project and Climate Change Knowledge Portal. Ordinary least squares (OLS) regression identified significant associations between climate factors and malaria outcomes but explained limited variance (adjusted $R^2 \leq 0.33$). Geographically Weighted Regression (GWR), however, revealed strong spatial heterogeneity, with local R^2 values often exceeding 0.7 and clear geographic contrasts in effect direction and strength. For instance, temperature effects were positive in West Africa but negative in Central and Southern regions, while rainfall showed opposite associations in eastern versus western Africa. These findings underscore the importance of spatially explicit models in climate–disease research and highlight the need for locally tailored malaria control strategies under future climate variability.

Keywords: Malaria, Climate variability, Temperature, Rainfall, Geographically Weighted Regression (GWR)

1. Introduction

Malaria is a life-threatening disease caused by the invasion of Plasmodium parasites into human red blood cells. It is primarily transmitted through the bite of infected female Anopheles mosquitoes, which serve as the dominant vectors. These mosquitoes are especially prevalent in sub-Saharan Africa, where malaria remains a major public health burden [1]. In 2021, the World Health Organization estimated approximately 247 million malaria cases and 619,000 related deaths worldwide, with the vast majority occurring in Africa [2].

Over the past few decades, significant progress has been made in malaria control through the use of insecticide-treated nets (ITNs), artemisinin-based combination therapies (ACTs), and indoor residual spraying (IRS) [3]. Despite these efforts, several critical limitations have hindered the long-term success of control strategies. First, mosquito vectors are increasingly developing resistance to commonly used insecticides due to overexposure in specific regions [4]. Second, access to malaria prevention tools remains limited in many communities due to economic barriers [5]. Third, complex

© 2025 The Authors. This is an open access article distributed under the terms of the Creative Commons Attribution License 4.0 (https://creativecommons.org/licenses/by/4.0/).

DOI: 10.54254/2753-8818/2025.AU27980

social structures—such as tribal governance—can challenge efforts in census-taking, outreach, and equitable tool distribution, thereby undermining intervention coverage [5].

To address these challenges, it is essential to understand the spatial patterns of malaria transmission so that prevention tools can be distributed more effectively with targeted government support. One of the key drivers of vector distribution is local climate, particularly temperature and precipitation [6,7]. These environmental variables shape mosquito breeding sites, survival rates, and parasite development. Mordecai et al. have discovered that temperature directly influences mosquito development speed, parasite incubation time, and vector survival, with optimal malaria transmission typically occurring between 25–28 °C [6]. Similarly, Q. Liu et al. analyzed data from 2000 to 2019 and found that increases in national annual average precipitation were associated with a 6.04% rise in the age-standardized incidence rate (ASIR) of malaria [7]. The impact of precipitation was notably significant in African countries, and children under five were the most affected age group.

Building on these findings, other studies have explored the combined and broader climatic influences on malaria transmission. Rice et al. discovered that extreme weather has interrupted malaria control activity, and increased incident rate of children within 3 months in 2022 and 2023 [8]. Abiodun et al. developed a climate-based mosquito-human malaria model to examine malaria dynamics in KwaZulu-Natal, South Africa, over several decades [9]. However, current researches on malaria-climate interactions faces three main limitations. First, studies usually assess temperature or precipitation independently, overlooking the interactive effects [10] between the two variables [6,7]. Second, most studies regarding Africa are country-specific, which may ignore regional interdependencies between neighboring countries that share ecological and epidemiological conditions [8,9]. Therefore, this study aims to investigate the combined influence of temperature and precipitation on malaria incidence across multiple African countries using a Geographically Weighted Regression (GWR) model [11]. This approach enables the identification of spatially varying relationships, while an interaction term between temperature and precipitation will be included to assess their mutual effects. Ultimately, this analysis seeks to provide a more nuanced understanding of climate-driven malaria transmission patterns, with implications for more efficient and regionally tailored intervention strategies.

2. Method

2.1. Study dataset

This study was based on a multi-country dataset that integrated national malaria surveillance indicators with annual climate variables for African countries between 2010 and 2015. The original dataset, gathered from Malaria Atlas Project (MAP) [12] and Climate Change Knowledge Portal (CCKP) [13], consisted of 522 records, each representing a specific country-year and malaria metric combination. For each row, the data includes the ISO 3 country code, country name, malaria indicators (incidence rate, mortality rate, and infection prevalence), year of observation, measurement unit, and corresponding metric value. All malaria metrics were standardized in units—cases per thousand population for incidence rate, cases per 100 thousand for mortality, and percentages per 100 children for infection prevalence— to ensure comparability across countries and years. In addition, each record contained climatic exposure information in the form of annual average temperature in Celsius and yearly total rainfall in millimeters, and geospatial coordinates (latitude and longitude) representing each country. To ensure data completeness and consistency for statistical analysis and spatial modelling, we adopted a complete-case strategy, excluding records with missing values in any key field. Specifically, 54 observations lacking temperature values, 72

DOI: 10.54254/2753-8818/2025.AU27980

missing rainfall data, and 18 with absent geographic coordinates were removed, resulting in a final analytic sample of 432 fully complete observations.

2.2. Data analysis

We calculated summary statistics (mean, standard deviation, range, and interquartile range) for all variables and visualized malaria data using histograms, box plots, time series plots, and scatter plots with OLS trend lines. Pearson correlation coefficients (ρ) were used to assess linear relationships between temperature, rainfall, and malaria metrics (incidence rate, mortality rate, infection prevalence), with two-tailed tests, 95% confidence intervals, t-statistics, and p-values reported. Analyses were stratified by malaria metric to reflect their distinct epidemiological meanings, while also checking for potential multicollinearity between climatic variables. This step both identified potential predictors and informed subsequent regression modeling. Building on these results, we specified four OLS regression models for each malaria outcome using R's lm() function: (1) temperature only, (2) rainfall only, (3) both predictors, and (4) both plus an interaction term (temperature × rainfall). All predictors were treated as continuous without transformation. Regression outputs included coefficients, standard errors, t-values, p-values, and adjusted R^2, and residual diagnostics were conducted to verify linearity, normality, and homoscedasticity. To formally evaluate the contribution of each predictor, ANOVA models were fitted using the aov() function: one with temperature only, one with rainfall only, and one full factorial model. ANOVA partitioned the total variance in malaria outcomes and used F-tests to determine the statistical significance of each term. This step was particularly important for assessing the interaction effect and determining whether the joint influence of temperature and rainfall differed from the sum of their individual effects. Together, the regression and ANOVA results provided a comprehensive understanding of the climatic drivers of malaria, clarifying whether effects were independent, additive, or interactive.

2.3. Geographically Weighted Regression

Recognizing that the relationship between climatic variables and malaria may not be spatially uniform, we applied Geographically Weighted Regression (GWR) to account for spatial heterogeneity in model coefficients. GWR extends traditional regression by allowing coefficients to vary across geographic locations, making it particularly suitable for analyzing spatially dependent health-environment relationships. For each of the three malaria metrics—incidence rate, mortality rate, and infection prevalence—we constructed three separate GWR models: a univariate model with temperature only, a univariate model with rainfall only, and a full model incorporating both variables along with their interaction term (temperature × rainfall). Each malaria observation was geo-located using country-level centroid coordinates (latitude and longitude), allowing us to model spatial variability across the African continent. GWR was implemented using a Gaussian kernel function with adaptive bandwidths to ensure that the effective number of neighbors varied depending on local data density. Bandwidth selection was data-driven and optimized using minimization of the corrected Akaike Information Criterion (AICc), providing a balance between local detail and model parsimony. After model fitting, local coefficient estimates were extracted for each location, capturing how the influence of climate on malaria varied spatially. These coefficients were converted into geospatial objects using the sf package and mapped onto country polygons. To aid interpretation at a national scale, we spatially aggregated the local coefficients by country borders, calculating the average temperature effect, rainfall effect, and interaction effect for each nation. The resulting choropleth maps were used to visualize spatial gradients in climate sensitivity, revealing

DOI: 10.54254/2753-8818/2025.AU27980

regional hotspots where malaria outcomes are more strongly associated with climatic factors. This spatially explicit analysis enhances understanding of how local ecological and environmental contexts mediate malaria transmission dynamics and provides valuable insight for geographically targeted public health interventions.

3. Result

The linear regression analysis showed that temperature and rainfall were significant predictors of disease metrics in most of the models. Yet, the overall explanatory power of these regressions was modest, with R^2 values ranging from 0.057 to 0.348. For example, rainfall accounted for only 14.7% of the variation in incidence rate ($R^2 = 0.147$), and even when combined with temperature, the explanatory power rose to just 33.6% ($R^2 = 0.336$). Similar patterns were observed for infection prevalence and mortality rate, both of which also displayed relatively low R^2 values, indicating that linear regression captured only a limited share of the variability. The ANOVA results supported these findings: temperature and rainfall had significant main effects ($p < 0.01$ in most cases), but their interaction was not significant ($p > 0.4$). This suggests that the influences of temperature and rainfall are largely independent. Detailed regression and ANOVA results are provided in the Supplementary Materials. Overall, these results indicate that simple linear regression does not fully account for the spatial heterogeneity in the climate–disease relationship, which motivated the use of geographically weighted regression (GWR) to examine local variation.

The geographically weighted regression (GWR) analysis of temperature and rainfall effects on malaria incidence, mortality, and infection prevalence revealed pronounced spatial heterogeneity across African countries (Figure 1). While the global OLS models estimated significant associations, their explanatory power was consistently low, with adjusted R^2 values often below 0.2. In contrast, GWR demonstrated substantially higher local fit in many countries, with R^2 values frequently exceeding 0.7 or even 0.9, underscoring the importance of accounting for spatial variation.

For malaria incidence, as shown in first row of Figure (1), the global OLS model indicated a significant positive association with temperature ($\beta = 18.48$, $p < 0.001$), but the explanatory power was low (adjusted $R^2 = 0.124$). In contrast, GWR highlighted substantial spatial variability. Strong positive temperature effects were observed in Benin ($\beta = 72.3$, $R^2 = 0.49$), Chad, the Central African Republic, Cameroon, and Nigeria. Some countries showed negative associations, most notably Equatorial Guinea ($\beta = -109.5$, $R^2 = 0.78$) and Gabon, while other nations such as Guinea-Bissau, Mozambique, and Zambia also exhibited negative trends. Botswana was an interesting case, with a near-zero coefficient ($\beta = 0.65$) but an exceptionally high local R^2 (0.96), indicating a strong local model fit despite minimal effect size. For malaria mortality, positive temperature effects were evident in Angola ($\beta = 15.7$, $R^2 = 0.60$) and several West African countries, including Chad, Benin, Liberia, Cameroon, the Central African Republic, and Nigeria. Negative associations were observed in Equatorial Guinea ($\beta = -22.8$, $R^2 = 0.79$), Gabon, Ghana, Guinea-Bissau, Mozambique, Zambia, and Zimbabwe. Similar spatial patterns emerged for malaria infection prevalence. Positive temperature effects were detected in Angola, Chad, Benin, Cameroon, and Liberia, whereas negative associations appeared in Equatorial Guinea, Gabon, Guinea-Bissau, Ghana, and Mozambique. These results highlight the pronounced context-dependence of temperature–malaria relationships, with both the direction and strength of effects varying considerably across countries.

DOI: 10.54254/2753-8818/2025.AU27980

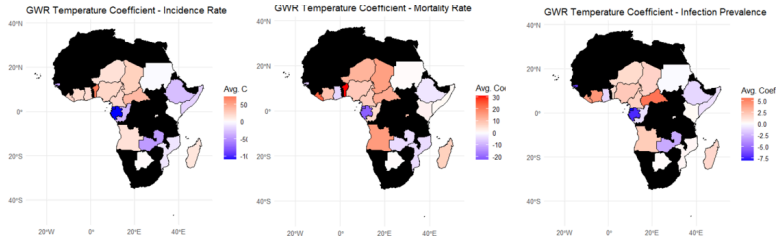

Figure 1. From left to right: (a), (b), (c).Spatial distribution of GWR temperature coefficients for malaria incidence rate, mortality rate, and infection prevalence across African countries. Countries in black indicate missing data

When examining the relationship between rainfall and malaria incidence, second row of Figure (1), GWR revealed notable regional contrasts. Strong positive associations appeared in several eastern and southern African countries, including Zimbabwe ($\beta = 0.176$, $R^2 = 0.86$), Ethiopia ($\beta = 0.166$, $R^2 = 0.49$), Mozambique ($\beta = 0.129$, $R^2 = 0.67$), and Somalia ($\beta = 0.137$, $R^2 = 0.73$). Moderate effects were also seen in Gabon, the Republic of Congo, Madagascar, and Kenya, with β values ranging from 0.004 to 0.114 and R^2 between 0.59 and 0.70. In contrast, several West and Central African countries—such as Nigeria, Benin, Zambia, Liberia, Cameroon, and Ivory Coast—exhibited negative coefficients ($\beta = -0.067$ to -0.006) and generally lower R^2 values, in some cases below 0.25. For malaria mortality rate, rainfall showed positive effects in Ghana ($\beta = 0.127$, $R^2 = 0.54$), Benin ($\beta = 0.121$, $R^2 = 0.62$), and Ivory Coast ($\beta = 0.123$, $R^2 = 0.32$), as well as in Mozambique, Nigeria, Cameroon, Liberia, and Rwanda, though with smaller β values. The Republic of the Congo stood out with a modest β (0.031) but a high R^2 (0.81), suggesting a consistent though relatively small effect. Negative or near-zero coefficients were recorded in Chad, Ethiopia, Kenya, Sudan, Zambia, and Zimbabwe, with R^2 values often under 0.10. For infection prevalence, positive rainfall associations emerged in Chad ($\beta = 0.018$, $R^2 = 0.67$) and Sudan ($\beta = 0.018$, $R^2 = 0.80$), alongside smaller yet consistently positive values in Angola, the Central African Republic, Mozambique, Botswana, Madagascar, Zimbabwe, Somalia, and the Republic of Congo. Here, R^2 values were frequently high, in several cases exceeding 0.70. Negative or negligible effects were observed in Nigeria, Liberia, Zambia, Ivory Coast, and Cameroon, typically accompanied by low explanatory power ($R^2 \leq 0.42$).

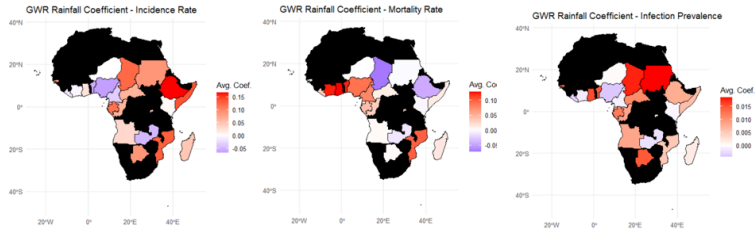

Figure 2. From left to right: (a), (b), (c). Spatial distribution of GWR rainfall coefficients for malaria incidence rate, mortality rate, and infection prevalence across African countries. Countries in black indicate missing data

When temperature, rainfall, and their interaction were modeled jointly, third row of Figure (1), GWR revealed substantial spatial heterogeneity in both effect sizes and explanatory power. Local R^2 values varied widely, from as low as 0.27 in Ghana to over 0.93 in Madagascar, indicating that the combined influence of climatic variables on malaria risk differs greatly between countries. Several nations in southern and eastern Africa showed strong positive associations for both temperature and

DOI: 10.54254/2753-8818/2025.AU27980

rainfall. For example, Madagascar (β_temp = 460, β_rain = 6.9, R^2 = 0.94), Zambia (β_temp = 573, β_rain = 13.1, R^2 = 0.60), and Somalia (β_temp = 93.3, β_rain = 4.0, R^2 = 0.86) showed consistently high local fit, suggesting that climatic drivers account for a large share of spatial variation in malaria outcomes there. Conversely, several countries exhibited negative coefficients for both variables, indicating that higher temperature or rainfall was associated with lower malaria metrics in those contexts. Notable examples include the Central African Republic (β_temp ≈ −206, β_rain = −5.1, R^2 = 0.67) and Mozambique (β_temp = −174, β_rain = −5.7, R^2 = 0.80). These areas may be influenced by ecological or socio-environmental factors that offset the expected climatic effects. Mixed patterns were also observed. In Equatorial Guinea (β_temp = 233, β_rain = 4.8, β_interaction = −0.19, R^2 = 0.71) and Benin (β_temp = 167, β_rain = 2.35, β_interaction = −0.08, R^2 = 0.49), temperature and rainfall effects were positive, yet their interaction term was negative, implying that simultaneous increases in both variables may not yield additive benefits. Comparable spatial contrasts were present for malaria mortality and infection prevalence under the joint climate model. Across metrics, GWR consistently produced high local R^2 values in certain regions while revealing opposite coefficient signs in others, underscoring that climate–malaria relationships are highly context-dependent and shaped by local environmental and epidemiological conditions.

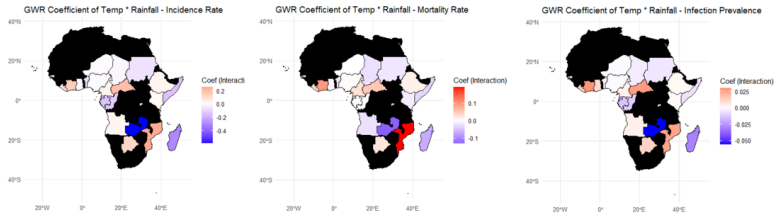

Figure 3. From left to right: (a), (b), (c). Spatial distribution of GWR temperature, rainfall, and their interaction coefficients for malaria incidence rate, mortality rate, and infection prevalence across African countries. Countries in black indicate missing data

Overall, the results indicate that while global OLS regressions show weak explanatory power for malaria-climate relationships, GWR shows much higher local R^2 values and strong spatial heterogeneity. The effects of temperature and rainfall and their interaction vary greatly across African countries, with both reinforcing and mitigating influences depending on local ecological and socio-environmental contexts. This underscores the importance of using spatially explicit models when examining climate–disease dynamics. Complete tables of GWR coefficients and local R^2 values for all countries are provided in the Supplementary Material, while the main text highlights representative countries to illustrate key spatial patterns.

4. Discussion

This study was conducted based on the GWR local regression model, and re-examined the hypotheses regarding the relationship between temperature, rainfall and malaria in the African region. Although the overall influence of climate variables was verified, their spatial heterogeneity was quite significant. The regression coefficients and their directions and intensities in the East Africa , West Africa, and southern Africa deviated from the overall average, suggesting that the climate-dominant pattern was reshaped by regional-specific factors.

Most importantly, in the East African region, extending from the Ethiopian Plateau southward to Kenya and Tanzania, the results of GWR present an extreme set of data. The temperature coefficient in this region is significantly higher or lower than the global average. For instance, the mortality rate

DOI: 10.54254/2753-8818/2025.AU27980

in Kenya (β_temp ≈13.41) and Rwanda(β_temp ≈-19.17). Meanwhile, the rainfall coefficient is close to zero or in the negative range, like in Ethiopia (β_rain ≈ -0.31). This pattern persists throughout the East African Rift Zone, where the Nubian Plate and the Somali Plate continue to separate, causing the land to rise above 1500 meters in altitude [14]. The resulting cooler air temperatures usually suppress malaria, but the steep cliffs and fault-controlled basins direct each convective storm towards rapid and high-energy runoff. Within hours, the bottom of the wide valleys and countless small depressions will be filled with temporary ponds, which will persist for days to weeks. The cause of this phenomenon may be attributed to the dominant small-scale agricultural economy characteristic of the East African region. Due to limited investment in drainage infrastructure, these ponds are rarely drained [15]. Therefore, in the East African large plate region, overall it indicates that the incidence of malaria is not particularly closely related to the average climate conditions of the region. The terrain and socio-economic environment have expanded the area of breeding grounds, resulting in an incidence rate exceeding the level that should be expected in this altitude zone solely determined by temperature and rainfall.

In West Africa, the surface of the region exhibits a consistent macroscopic feature: the temperature coefficient throughout the entire area consistently shows a significant positive value, while the rainfall coefficient is generally negative, for example, Nigeria fits this result (β_temp ≈7.49, β_rain ≈ -0.06). This coherent pattern depicts the vast, low-lying West Africa and its extensive coastal plains, where the hot low-pressure system of the Sahara and the monsoon of Guinea usually bring high temperatures and high humidity [16]. However, over the past two decades, large-scale state-led irrigation projects have transformed approximately 12,000 square kilometers of savanna grasslands and floodplains [17] into permanent rice fields and small reservoirs. The resulting artificial wetlands effectively isolate the breeding of mosquitoes from natural rainfall, forming stable water layers under persistently high-temperature air. Therefore, in the entire West African region, the surface coefficients collectively indicate that the incidence of malaria is more influenced by the density of human-managed water bodies and persistence rather than annual rainfall, thereby generating significant abnormal high incidence phenomena in regions with originally unfavorable climatic conditions.

In the southern African region, from the Limpo River Basin to Cape Town, the temperature coefficient has consistently shown a negative trend, like Botswana (β_temp ≈-9.31) and the interaction term further weakened the influence of the overall climate signal. This extensive negative area is highly associated with the stability and gently undulating plateaus of the South African region. There, warm and humid summers should be conducive to the spread of malaria. However, the economic situation in this region has changed the risk profile: the dense urban layout in South Africa and widespread use of air conditioning have reduced the contact between humans and mosquitoes [18]. In most areas, the increasing domestic and international funds have been invested in regular indoor spraying and large-scale distribution of mosquito nets, expanding the coverage to previously remote villages [19,20]. At the same time, the main vector in the South African region has quietly shifted from the Gambian anopheles to the more drought-tolerant Fenschstes anopheles, which narrows the breeding window and reduces the number of adult mosquitoes in any rainfall event. Overall, these economic, infrastructure, and ecological buffering factors have overcome the influence of climate factors, so the current recorded malaria incidence in South Africa is much lower than the level predicted solely by temperature and rainfall [21].

DOI: 10.54254/2753-8818/2025.AU27980

5. Limitation

While this study provides important insights, a few considerations should be kept in mind. Data coverage across African countries is uneven, as health surveillance systems remain limited in some regions, particularly in areas affected by conflict or fragile governance. This meant our analysis could focus only on countries with more complete records, making the identified patterns indicative rather than continent-wide. Similarly, reliance on country-level climate averages may overlook important subnational variations, given Africa's diverse ecological zones. Finally, although the GWR model highlights valuable spatial associations between climate and malaria, these patterns should be interpreted as part of a broader context where demographic, economic, and health system factors also play key roles, which most current studies also struggles to do.

6. Conclusion

The study demonstrates that malaria transmission in Africa is closely shaped by climatic factors, but in highly localized and context-dependent ways. While global OLS models revealed only weak associations between temperature, rainfall, and malaria outcomes, the use of Geographically Weighted Regression (GWR) uncovered substantial spatial heterogeneity, with local explanatory power frequently exceeding 0.7. These findings highlight the importance of spatially explicit approaches when studying climate–disease dynamics, as national or continental averages risk obscuring meaningful subnational patterns.

Our results show that regions such as the East African Rift, West Africa, and southern Africa exhibit distinct climate–malaria relationships that reflect the interaction of ecological, hydrological, and socioeconomic factors. For example, temporary waterlogging in the Rift Valley amplifies malaria risk even under mild temperatures [14,15], while artificial irrigation projects in West Africa have created high-incidence hotspots despite low rainfall [16,17]. Conversely, strong prevention efforts and changing mosquito ecology in southern Africa appear to suppress climate-driven risks, underscoring the power of targeted interventions [19,20]. Together, these patterns emphasize that climate alone does not determine malaria outcomes; rather, it interacts with human and ecological systems in complex ways.

While data availability and reliance on country-level climate averages remain constraints, and causal mechanisms cannot be fully inferred from this analysis, the GWR framework nonetheless provides valuable insights. By identifying where and how climate variables most strongly correlate with malaria outcomes, this study offers a foundation for regionally tailored strategies that combine environmental monitoring with targeted control measures. Ultimately, advancing malaria control in Africa will require not only strengthening health surveillance and incorporating finer-grained climate data, but also integrating interventions with the unique ecological and socioeconomic contexts of each region.

References

[1] B. St. Laurent, "Mosquito vector diversity and malaria transmission, " Frontiers in Malaria, vol. 3, Art. 1600850, 2025, doi: 10.3389/fmala.2025.1600850.

[2] UNICEF, "Malaria, " UNICEF Data. [Online]. Available: https: //data.unicef.org/topic/child-health/malaria/. [Accessed: Aug. 23, 2025].

[3] J. Hemingway et al., "Averting a malaria disaster: Will insecticide resistance derail malaria control?, " The Lancet, vol. 387, no. 10029, pp. 1785–1788, 2016, doi: 10.1016/S0140-6736(15)00417-1.

[4] M. C. Reid and F. E. McKenzie, "The contribution of agricultural insecticide use to increasing insecticide resistance in African malaria vectors, " Malaria Journal, vol. 15, p. 107, 2016, doi: 10.1186/s12936-016-1162-4.

DOI: 10.54254/2753-8818/2025.AU27980

[5] R. Ratcliffe, “Malaria cases rise for fifth year as disasters and resistance hamper control efforts, ” The Guardian, Dec. 11, 2024. [Online]. Available: https: //www.theguardian.com/global-development/2024/dec/11/global-health-deaths-malaria-rise-drug-insecticide-resistance-climate-crisis-funding-un.
[6] E. A. Mordecai et al., “Optimal temperature for malaria transmission is dramatically lower than previously predicted, ” Ecology Letters, vol. 16, no. 1, pp. 22–30, 2013, doi: 10.1111/ele.12015.
[7] E. I. Obeagu and G. U. Obeagu, “Adapting to the shifting landscape: Implications of climate change for malaria control: A review, ” Medicine, vol. 103, no. 29, e39010, 2024, doi: 10.1097/MD.0000000000039010.
[8] B. L. Rice et al., “Vaccination to mitigate climate-driven disruptions to malaria control in Madagascar, ” Science, vol. 389, no. 6757, pp. 257–262, 2025, doi: 10.1126/science.adp5365.
[9] G. J. Abiodun, P. J. Witbooi, K. O. Okosun, and R. Maharaj, “Exploring the impact of climate variability on malaria transmission using a dynamic mosquito–human malaria model, ” Infectious Diseases of Poverty, vol. 8, no. 1, p. 40, 2019, doi: 10.1186/s40249-019-0550-5.
[10] V. Jain, S. Kumar, and M. K. Goyal, “Relationship between daily precipitation extremes and temperature in changing climate across smart cities of Central India, ” Journal of Environmental Management, vol. 380, 125036, 2025, doi: 10.1016/j.jenvman.2025.125036.
[11] W. R. Tobler, “A comparison of simulated and observed spatial interaction in the United States, ” Geographical Analysis, vol. 28, no. 1, pp. 1–20, 1996, doi: 10.1111/j.1538-4632.1996.tb00936.x.
[12] Malaria Atlas Project, “Analytics for a malaria-free world.” [Online]. Available: https: //malariaatlas.org. [Accessed: Sep. 4, 2025].
[13] The World Bank Group, “Climate Change Knowledge Portal.” [Online]. Available: https: //climateknowledgeportal.worldbank.org/. [Accessed: Sep. 4, 2025].
[14] C. J. Ebinger and C. A. Scholz, “Continental rift basins: The East African perspective, ” Geological Society, London, Special Publications, vol. 427, no. 1, pp. 3–20, 2012, doi: 10.1144/SP427.2.
[15] Agricultural Policy Research in Africa (APRA), “Agricultural commercialisation and rural livelihoods in Malawi: A historical and contemporary agrarian inquiry, ” Future Agricultures Consortium, 2020. [Online]. Available: https: //www.future-agricultures.org/apra/publications/working-papers/.
[16] USAID, “Guinea country development cooperation strategy, ” 2021. [Online]. Available: https: //www.climatelinks.org/sites/default/files/asset/document/2021-03/2021_USAID_CDCS-Annex-Guinea.pdf.
[17] A. Diagne, P. Séréme, M. Konaté, and D. Fargette, “Rivers and landscape ecology of Rice yellow mottle virus along the Niger Valley, ” HAL Open Science, 2006. [Online]. Available: https: //hal.science/hal-03365735.
[18] A. Kolimenakis, S. Heinz, M. L. Wilson, and O. Horstick, “Urbanization and the mosquito population: Threats to human health, ” ResearchGate, 2023, doi: 10.13140/RG.2.2.12345.67890.
[19] B. G. Damien et al., “Long-lasting insecticide-treated nets combined or not with indoor residual spraying may not be sufficient to eliminate malaria: A case-control study, Benin, West Africa, ” Tropical Medicine and Infectious Disease, 2023, doi: 10.3390/tropicalmed8100475.
[20] A. K. Mishra et al., “Improvement of indoor residual spraying and long-lasting insecticidal net services through structured monitoring and supervision as part of the Malaria Elimination Demonstration Project in Mandla, Madhya Pradesh, ” Malaria Journal, 2021, doi: 10.1186/s12936-021-03639-9.
[21] B. D. Brooke, J. Raman, J. Frean, F. Ridl, and B. Sharp, “Malaria vectors and vector surveillance in Limpopo Province (South Africa): 1927 to 2018, ” International Journal of Environmental Research and Public Health, 2020, doi: 10.3390/ijerph17114125.

DOI: 10.54254/2753-8818/2025.AU27980

Supporting materials

Table 1. Linear regression results for the effect of temperature and rainfall on disease metrics

Metric	Predictor	Estimate	Std. Error	t value	p value	R^2
Incidence Rate	Temperature	18.480	4.036	4.579	9.83e-06 ***	0.124
	Rainfall	0.0806	0.0160	5.048	1.29e-06 ***	0.147
	Combined	24.431	9.406	2.597	0.0104 *	0.336
Infection Prevalence	Temperature	1.824	0.431	4.232	4.04e-05 ***	0.108
	Rainfall	0.0092	0.0017	5.548	1.29e-07 ***	0.172
	Combined	1.831	0.986	1.856	0.0655	0.348
Mortality Rate	Temperature	9.807	1.620	6.053	1.12e-08 ***	0.198
	Rainfall	0.0211	0.0070	2.992	0.0032 **	0.057
	Combined	14.358	4.019	3.572	0.00048 ***	0.312

Significance codes: *** $p < 0.001$, ** $p < 0.01$, * $p < 0.05$, . $p < 0.1$

Table 2. ANOVA results for effects of temperature, rainfall, and their interaction

Metric	p value (Temperature)	p value (Rainfall)	p value (Interaction)
Incidence Rate	9.83e-06 ***	1.29e-06 ***	0.893
Infection Prevalence	4.04e-05 ***	1.29e-07 ***	0.562
Mortality Rate	1.12e-08 ***	0.0032 **	0.404

Table 3-5: Geographically Weighted Regression (GWR) results for malaria indicators across countries.

Table 3. Incidence rate

Country	Temperature Model	Rainfall Model	Interaction Model
Angola	17.112 (-207.42, R^2=0.42)	0.032 (128.96, R^2=0.07)	-1.343, -0.694, 0.025 (350.50, R^2=0.81)
Benin	72.297 (-1667.21, R^2=0.49)	-0.056 (424.97, R^2=0.23)	167.054, 2.347, -0.083 (-4353.88, R^2=0.49)
Botswana	0.650 (-13.07, R^2=0.96)	0.089 (-34.61, R^2=0.82)	-40.285, -2.503, 0.118 (846.84, R^2=0.81)
Cameroon	20.777 (-246.41, R^2=0.69)	-0.036 (337.24, R^2=0.44)	-6.137, -0.738, 0.032 (333.07, R^2=0.74)
Central African Republic	38.955 (-612.89, R^2=0.45)	0.063 (292.21, R^2=0.54)	-205.861, -5.104, 0.194 (5832.34, R^2=0.67)
Chad	25.914 (-503.62, R^2=0.77)	0.122 (172.73, R^2=0.41)	42.846, 0.824, -0.024 (-1027.45, R^2=0.85)
Equatorial Guinea	-109.537 (2996.13, R^2=0.78)	0.088 (81.92, R^2=0.59)	232.760, 4.809, -0.193 (-5539.95, R^2=0.71)
Ethiopia	-30.293 (840.35, R^2=0.40)	0.166 (-20.40, R^2=0.49)	-42.664, -0.738, 0.030 (1152.88, R^2=0.55)

DOI: 10.54254/2753-8818/2025.AU27980

Table 3. (continued)

Gabon	-110.078 (2983.93, R^2=0.84)	0.114 (9.58, R^2=0.63)	160.034, 3.654, -0.145 (-3833.28, R^2=0.80)
Ghana	18.464 (-165.43, R^2=0.11)	0.023 (322.85, R^2=0.08)	49.422, 0.437, -0.013 (-1102.30, R^2=0.27)
Guinea-Bissau	-45.655 (1394.95, R^2=0.48)	0.078 (-17.97, R^2=0.61)	16.951, 0.923, -0.032 (-413.99, R^2=0.76)
Ivory Coast	19.358 (-177.99, R^2=0.04)	-0.006 (348.12, R^2=0.02)	-172.569, -3.780, 0.148 (4728.87, R^2=0.32)
Kenya	0.044 (67.73, R^2=0.37)	0.004 (65.70, R^2=0.59)	-17.158, -0.381, 0.015 (494.35, R^2=0.71)
Liberia	22.788 (-271.13, R^2=0.22)	-0.016 (352.12, R^2=0.22)	-147.698, -2.251, 0.086 (4223.01, R^2=0.48)
Madagascar	13.018 (-206.67, R^2=0.15)	0.048 (22.59, R^2=0.70)	459.602, 6.938, -0.301 (-10501.08, R^2=0.94)
Mozambique	-10.342 (615.63, R^2=0.34)	0.129 (239.29, R^2=0.67)	-173.550, -5.664, 0.254 (4076.60, R^2=0.80)
Niger	15.431 (-95.75, R^2=0.40)	0.000 (341.32, R^2=0.07)	16.769, 0.036, -0.001 (-133.61, R^2=0.45)
Nigeria	22.998 (-306.97, R^2=0.56)	-0.067 (397.42, R^2=0.39)	54.023, 0.411, -0.013 (-1230.43, R^2=0.70)
Republic of the Congo	-32.968 (1034.39, R^2=0.79)	0.065 (106.57, R^2=0.62)	150.760, 3.077, -0.121 (-3626.68, R^2=0.81)
Rwanda	7.882 (-92.66, R^2=0.17)	0.042 (7.01, R^2=0.35)	-11.883, -0.420, 0.024 (236.21, R^2=0.51)
Somalia	-19.825 (577.38, R^2=0.46)	0.137 (3.58, R^2=0.73)	93.309, 3.959, -0.149 (-2456.92, R^2=0.86)
Sudan	-0.596 (52.34, R^2=0.31)	0.089 (12.75, R^2=0.56)	17.020, 1.853, -0.065 (-448.69, R^2=0.81)
Zambia	-46.512 (1228.31, R^2=0.36)	-0.049 (249.65, R^2=0.21)	573.033, 13.118, -0.593 (-12467.93, R^2=0.60)
Zimbabwe	-29.897 (820.53, R^2=0.84)	0.176 (-33.90, R^2=0.86)	2.628, 0.992, -0.036 (-65.78, R^2=0.91)

Table 4. Mortality rate

Country	Temperature Model	Rainfall Model	Interaction Model
Angola	15.683 (-303.83, R^2=0.60)	0.003 (32.23, R^2=0.00)	41.643, 0.543, -0.023 (-903.51, R^2=0.76)
Benin	30.836 (-750.15, R^2=0.38)	0.121 (1.06, R^2=0.62)	48.895, 0.562, -0.019 (-1279.40, R^2=0.40)
Botswana	0.104 (-2.10, R^2=0.68)	0.002 (-0.65, R^2=0.31)	-9.309, -0.549, 0.025 (201.13, R^2=0.85)
Cameroon	7.550 (-84.44, R^2=0.40)	0.077 (-16.99, R^2=0.28)	-28.385, -0.755, 0.030 (824.85, R^2=0.57)
Central African Republic	13.450 (-230.62, R^2=0.56)	0.010 (98.94, R^2=0.00)	-57.449, -1.387, 0.053 (1620.93, R^2=0.81)
Chad	15.096 (-363.73, R^2=0.76)	-0.073 (83.09, R^2=0.05)	24.313, 0.677, -0.023 (-630.66, R^2=0.81)
Equatorial Guinea	-22.750 (638.81, R^2=0.79)	0.004 (68.48, R^2=0.30)	58.565, 1.000, -0.040 (-1388.20, R^2=0.83)

DOI: 10.54254/2753-8818/2025.AU27980

Table 4. (continued)

Ethiopia	-2.988 (84.70, R^2=0.12)	-0.044 (52.55, R^2=0.08)	-12.567, -0.309, 0.011 (344.42, R^2=0.34)
Gabon	-21.123 (593.40, R^2=0.76)	0.041 (-15.49, R^2=0.79)	-3.283, -0.001, 0.001 (89.71, R^2=0.86)
Ghana	-5.032 (250.64, R^2=0.24)	0.127 (-49.60, R^2=0.54)	6.216, 0.213, -0.006 (-98.83, R^2=0.42)
Guinea-Bissau	-7.411 (241.98, R^2=0.24)	0.001 (32.19, R^2=0.00)	28.657, 0.597, -0.021 (-780.62, R^2=0.69)
Ivory Coast	9.648 (-126.68, R^2=0.15)	0.123 (-21.31, R^2=0.32)	-141.030, -2.539, 0.098 (3806.58, R^2=0.51)
Kenya	1.801 (-36.78, R^2=0.13)	-0.003 (10.69, R^2=0.01)	13.410, 0.342, -0.014 (-329.59, R^2=0.40)
Liberia	23.334 (-489.28, R^2=0.41)	0.031 (28.19, R^2=0.29)	-49.615, -0.950, 0.036 (1429.95, R^2=0.59)
Madagascar	7.298 (-138.70, R^2=0.26)	0.014 (8.42, R^2=0.37)	110.971, 1.601, -0.069 (-2533.94, R^2=0.96)
Mozambique	-4.594 (209.66, R^2=0.01)	0.097 (4.55, R^2=0.10)	-134.187, -4.315, 0.192 (3010.22, R^2=0.47)
Niger	11.910 (-158.65, R^2=0.16)	0.000 (178.70, R^2=0.00)	13.227, 0.009, -0.000 (-195.79, R^2=0.25)
Nigeria	8.322 (-106.21, R^2=0.32)	0.089 (21.06, R^2=0.24)	7.488, -0.062, 0.003 (-110.49, R^2=0.53)
Republic of the Congo	5.447 (-82.49, R^2=0.66)	0.031 (2.32, R^2=0.81)	1.888, 0.031, 0.000 (-44.36, R^2=0.92)
Rwanda	9.749 (-155.78, R^2=0.29)	0.035 (-11.54, R^2=0.29)	-19.169, -0.441, 0.024 (369.66, R^2=0.51)
Somalia	0.651 (-7.66, R^2=0.12)	0.011 (6.84, R^2=0.01)	20.595, 0.834, -0.032 (-536.06, R^2=0.75)
Sudan	0.136 (3.00, R^2=0.08)	-0.003 (7.53, R^2=0.02)	4.738, 0.495, -0.018 (-126.61, R^2=0.87)
Zambia	-4.538 (134.84, R^2=0.15)	-0.014 (48.33, R^2=0.05)	132.074, 2.905, -0.131 (-2886.43, R^2=0.51)
Zimbabwe	-2.731 (76.76, R^2=0.58)	-0.000 (2.97, R^2=0.00)	-0.778, 0.064, -0.002 (23.20, R^2=0.77)

Table 5. Infection prevalence

Country	Temperature Model	Rainfall Model	Interaction Model
Angola	2.124 (-34.87, R^2=0.65)	0.008 (2.43, R^2=0.53)	-1.879, -0.104, 0.004 (68.46, R^2=0.88)
Benin	1.328 (-2.68, R^2=0.20)	0.015 (18.94, R^2=0.31)	7.933, 0.083, -0.002 (-211.96, R^2=0.44)
Botswana	0.126 (-2.72, R^2=0.98)	0.015 (-5.87, R^2=0.77)	-4.170, -0.254, 0.012 (88.31, R^2=0.79)
Cameroon	1.866 (-23.18, R^2=0.62)	-0.001 (26.47, R^2=0.42)	-1.045, -0.086, 0.004 (36.47, R^2=0.69)
Central African Republic	5.533 (-101.64, R^2=0.52)	0.011 (24.12, R^2=0.60)	-26.856, -0.724, 0.028 (745.96, R^2=0.64)
Chad	1.734 (-32.35, R^2=0.67)	0.018 (9.39, R^2=0.67)	5.822, 0.132, -0.004 (-152.79, R^2=0.83)
Equatorial Guinea	-8.118 (226.95, R^2=0.64)	0.009 (6.74, R^2=0.51)	21.382, 0.449, -0.018 (-510.81, R^2=0.62)
Ethiopia	-1.351 (37.60, R^2=0.43)	0.008 (-0.98, R^2=0.55)	-1.331, -0.032, 0.001 (34.95, R^2=0.50)
Gabon	-7.342 (204.68, R^2=0.72)	0.012 (-1.56, R^2=0.59)	16.372, 0.360, -0.014 (-396.70, R^2=0.73)
Ghana	-1.243 (70.99, R^2=0.05)	0.016 (17.96, R^2=0.07)	-7.648, -0.234, 0.010 (211.77, R^2=0.37)
Guinea-Bissau	-6.781 (197.34, R^2=0.73)	0.014 (-16.05, R^2=0.73)	4.775, 0.145, -0.005 (-131.47, R^2=0.87)

DOI: 10.54254/2753-8818/2025.AU27980

Table 5. (continued)

Ivory Coast	4.292 (-78.48, R^2=0.07)	-0.001 (38.17, R^2=0.04)	-32.882, -0.765, 0.030 (865.19, R^2=0.44)
Kenya	0.184 (0.28, R^2=0.40)	-0.001 (5.38, R^2=0.60)	-1.395, -0.034, 0.001 (39.61, R^2=0.70)
Liberia	4.030 (-72.01, R^2=0.21)	-0.003 (39.01, R^2=0.19)	-22.368, -0.370, 0.014 (621.90, R^2=0.52)
Madagascar	1.533 (-29.47, R^2=0.48)	0.002 (3.18, R^2=0.88)	46.193, 0.702, -0.031 (-1057.07, R^2=0.96)
Mozambique	0.282 (26.85, R^2=0.67)	0.005 (28.69, R^2=0.92)	-17.595, -0.572, 0.025 (415.27, R^2=0.83)
Niger	1.427 (-14.60, R^2=0.42)	0.000 (25.79, R^2=0.25)	1.795, 0.018, -0.001 (-25.05, R^2=0.47)
Nigeria	2.165 (-31.24, R^2=0.49)	-0.004 (32.53, R^2=0.39)	5.359, 0.036, -0.001 (-129.91, R^2=0.64)
Republic of the Congo	-1.006 (43.87, R^2=0.73)	0.008 (4.70, R^2=0.69)	14.415, 0.279, -0.011 (-351.88, R^2=0.80)
Rwanda	0.470 (-5.81, R^2=0.31)	0.001 (2.13, R^2=0.61)	-0.688, -0.029, 0.002 (13.65, R^2=0.63)
Somalia	-0.922 (27.03, R^2=0.48)	0.006 (0.44, R^2=0.70)	4.329, 0.167, -0.006 (-114.74, R^2=0.80)
Sudan	-0.156 (6.36, R^2=0.81)	0.018 (-2.73, R^2=0.80)	1.295, 0.145, -0.005 (-35.78, R^2=0.89)
Zambia	-2.875 (79.20, R^2=0.33)	-0.002 (17.83, R^2=0.39)	55.093, 1.240, -0.056 (-1198.25, R^2=0.58)
Zimbabwe	-1.424 (38.99, R^2=0.84)	0.008 (-1.69, R^2=0.86)	0.243, 0.049, -0.002 (-6.43, R^2=0.89)